J|A|C|S
ARTICLES

Published on Web 04/14/2010

Effect of a Strong Interfacial Electric Field on the Orientation of the Dipole Moment of Thiolated Aib-Oligopeptides Tethered to Mercury on Either the N- or C-Terminus

Lucia Becucci,*,† Ivan Guryanov,‡ Flavio Maran,‡ and Rolando Guidelli†

Department of Chemistry, Florence University, Via della Lastruccia 3, 50019 Sesto Fiorentino, Firenze, Italy, and Department of Chemistry, University of Padova, Via Marzolo 1, 35131 Padova, Italy

Received January 19, 2010; E-mail: lucia.becucci@unifi.it

Abstract: Four oligopeptides consisting of a sequence of α-aminoisobutyric acid (Aib) residues, thiolated at either the N- or C-terminus by means of a $-(CH_2)_2-SH$ anchor, were self-assembled on mercury, which is a substrate known to impart a high fluidity to self-assembled monolayers (SAMs). The surface dipole potential of these peptide SAMs was estimated in 0.1 M KCl aqueous solution at a negatively charged electrode, where the interfacial electric field is directed toward the metal. To the best of our knowledge, this is the first estimate of the surface dipole potential of peptide SAMs in aqueous solution. The procedure adopted consisted in measuring the charge involved in the gradual expansion of a peptide-coated mercury drop and then combining the resulting information with an estimate of the charge density experienced by diffuse layer ions. The dipole moment of the tethered thiolated peptides was found to be directed toward the metal, independent of whether they were thiolated at the C- or N-terminus. This result was confirmed by the effect of these SAMs on the kinetics and thermodynamics of the Eu(III)/Eu(II) redox couple. The combined outcome of these studies indicates that a strong interfacial electric field orients the dipole moment of peptide SAMs tethered to mercury, even against their "natural" dipole moment.

1. Introduction

Electron-transfer (ET) reactions in a biological system occur through a sequence of steps involving redox moieties surrounded by a polypeptide matrix. It is generally believed that these polypeptides act as efficient mediators of electron tunneling.[1] In addition, the large dipole moment that develops along helical peptides[2] is thought to facilitate ET if properly positioned with respect to the electron tunneling pathway. To clarify this aspect, both photoinduced and electrochemically induced ETs along helical peptides have been extensively investigated.[3]

Surface dipole potential values of organic layers on metal surfaces have been extracted from changes of the metal work function upon formation of these layers by the Kelvin probe method, either in vacuo[4,5] or in atmosphere,[6] and by photoelectron spectroscopy.[5,7] These measurements have been normally carried out on self-assembled monolayers (SAMs) of simple or functionalized alkanethiols. In what follows, the surface dipole potential is taken as positive when the dipoles point their positive pole toward the metal; moreover, a dipole moment is regarded as positive when directed from the negative to the positive pole. Evans and Ulman[6] found that the dipole potential of *n*-alkanethiols anchored to gold varies linearly with increasing chain length. By assuming that each additional methylene unit does not contribute any additional net dipole moment to that already existing in the molecule, they concluded that the dielectric constant should decrease as the chain length increases. This assumption implies ignoring the possibility for the protons resulting from the deprotonation of the sulfhydryl groups following thiol adsorption to be located at the distal end of the alkyl chain. By using the Kelvin probe method, Imanishi et al.[4] estimated, under high-vacuum conditions, the change of the surface dipole potential of gold upon adsorption of helical peptides. The peptide chains consisted of an alternating sequence of alanine (Ala) and α-aminoisobutyric acid (Aib) residues. To form the SAM on gold, a lipoic acid moiety, with its disulfide group, was covalently linked either to the C- or the N-terminus

† Florence University.
‡ University of Padova.

(1) (a) Skourtis, S. S.; Beratan, D. N. *Adv. Chem. Phys.* **1999**, *106*, 377. (b) Gray, H. B.; Winkler, J. R. In *Electron Transfer in Chemistry*; Balzani, V., Ed.;,Wiley-VCH: Weinheim, 2001; Vol. 1, p 3. (c) Long, Y. T.; Abu-Irhayem, E.; Kraatz, H.-B. *Chem.—Eur. J.* **2005**, *11*, 5186–5194. (d) Cordes, M.; Giese, B. *Chem. Soc. Rev.* **2009**, *38*, 892–901.
(2) Shin, Y.-G.; Newton, M. D.; Isied, S. S. *J. Am. Chem. Soc.* **2003**, *125*, 3722–3732.
(3) (a) Fox, M. A.; Galoppini, E. *J. Am. Chem. Soc.* **1997**, *119*, 5277–5285. (b) Galoppini, E.; Fox, M. A. *J. Am. Chem. Soc.* **1996**, *118*, 2299–2300. (c) Morita, T.; Kimura, S.; Kobayashi, S.; Imanishi, Y. *J. Am. Chem. Soc.* **2000**, *122*, 2850–2859. (d) Yasutomi, S.; Morita, T.; Imanishi, Y.; Kimura, S. *Science* **2004**, *304*, 1944–1947. (e) Yasutomi, S.; Morita, T.; Kimura, S. *J. Am. Chem. Soc.* **2005**, *127*, 14564–14565. (f) Sek, S.; Tolak, A.; Misicka, A.; Palys, B.; Bilewicz, R. *J. Phys. Chem. B* **2005**, *109*, 18433–18438. (g) Sek, S.; Swiatek, K.; Misicka, A. *J. Phys. Chem. B* **2005**, *109*, 23121–23124.
(4) Imanishi, Y.; Miura, Y.; Iwamoto, M.; Kimura, S.; Umemura, J. *Proc. Jpn. Acad. Ser. B* **1999**, *75*, 287–290.
(5) Ray, S. G.; Cohen, H.; Naaman, R.; Liu, H.; Waldeck, D. H. *J. Phys. Chem. B* **2005**, *109*, 14064–14073.
(6) Evans, S. D.; Ulman, A. *Chem. Phys. Lett.* **1990**, *170*, 462–466.
(7) Alloway, D. M.; Hofmann, M.; Smith, D. L.; Gruhn, N. E.; Graham, A. L.; Colorado, R., Jr.; Wysocki, V. H.; Lee, T. R.; Lee, P. A.; Armstrong, N. R. *J. Phys. Chem. B* **2003**, *107*, 11690–11699.

10.1021/ja100486y

of the peptide chain. The surface dipole potential of the peptides anchored to gold on the N-terminus side was found to be positive and to increase linearly with the chain length. On the other hand, the surface dipole potential of the peptides anchored at the C-terminus was negative, but it did not show such a proportionality. Naaman and co-workers[5] compared the dipole moments of a number of thiolated organic molecules, estimated from work function measurements on gold-supported monolayers, with those obtained from ab initio calculations of the isolated molecules. They concluded that ET between the metal substrate and the monolayer is small for adsorbed molecules pointing their dipole toward the metal surface. Conversely, ET from the metal to the molecule is appreciable for adsorbed molecules pointing their dipole away from the metal surface; with one particular molecule, the charge transfer was even found to be large enough to invert the direction of the dipole.

Galoppini and Fox[3b] were the first to address the issue of whether the dipole moment of peptides with an alternating Ala-Aib backbone could affect the photoinduced ET from a neutral donor D to a neutral acceptor A. To this end, D and A were appended, in the order, along the peptide chain either in the direction of the peptide dipole moment or in the opposite direction. The rate constant for photoinduced electron transfer was found to be larger with the former arrangement. This is in agreement with the fact that, for stable helices, ET is facilitated when electron tunneling occurs in the direction of the dipole moment, i.e., when the helix stabilizes the resulting charge separation state. In keeping with this hypothesis, the same authors observed that unfolding the helical peptide with a protic solvent could reduce such a difference in rate constants very significantly.[3a] An analogous approach was followed by other groups to assess the influence of the surface dipole potential of helical peptides on electrochemically induced ET. To this end, a disulfide[8] or sulfhydryl group[3f,9] was linked to the C-terminus of a helical peptide and an electro-oxidazable ferrocene (Fc) moiety at its N-terminus, or vice versa. The helix content of the peptides was estimated from circular dichroism (CD) spectra, whereas the amide I/amide II absorbance ratio of infrared reflection absorption spectroscopy (IRRAS) spectra provided information on the tilt of the helix axis relative to the substrate.[8c] By using a peptide with a leucine (Leu)-Aib backbone tethered to gold via a lipoic acid moiety, the Fc electroxidation rate constant was found to be higher when the surface dipole potential of the peptide was positive than when it was negative.[8a] It was concluded that ET from Fc to gold is favored by a dipole moment directed toward the metal. A similar system was also examined by scanning tunneling spectroscopy.[8d] Conversely, the same group found that a different Ala-Aib-based peptide did not show any appreciable difference in rate constant value by reversing the direction of the peptide dipole potential. This behavior was justified by ascribing the rate-determining step to the ET across the lipoic acid linker.[8b]

Mandal and Kraatz[9a] prepared a leucine-rich peptide with a cysteine residue at the C-terminus and a Fc moiety at the N-terminus and diluted it with a large amount of the same peptide with no Fc; the resulting mixture was tethered to a gold electrode. The kinetic behavior of this monolayer was compared with that of a monolayer in which one-half of the above Fc-free peptide was replaced by a Fc-free peptide with the cysteine residue at the N-terminus. The negative surface dipole potential in the first monolayer should slow the ET from Fc to the metal (i.e., Fc electro-oxidation) and accelerate the ET in the opposite direction with respect to the second monolayer, in which the net surface dipole potential is practically zero. Both effects are expected to shift the formal potential of the Fc/Fc^+ redox couple of the first monolayer in the positive direction. In fact, the formal potential in the first monolayer was found to be more positive than that in the second monolayer by ~50 mV. The authors provided a different explanation for this behavior. The opposing effect of the negative surface dipole potential of an alanine-rich peptide on Fc oxidation and on Fc^+ reduction was pointed out by Sek et al.,[3f] by calculating an anodic charge-transfer coefficient lower than the cathodic one. Morita et al.[3c] verified the influence of the surface dipole potential of helical peptides on photoelectrochemically induced electron transfer. A lipoic acid residue was linked to the C-terminus of an (Ala-Aib)-based peptide and a chromophore donor to its N-terminus, or vice versa. The chromophore was photoexcited in the presence of an acceptor in solution, giving rise to a cathodic photocurrent whose quantum efficiency was higher for the peptide with negative surface dipole potential. This approach was used to fabricate a molecular photodiode composed of two types of peptides carrying different chromophores and having opposing dipole moments.[3d]

To the best of our knowledge, the surface dipole potential of SAMs of helical peptides in aqueous solution has never been estimated. Recently, we devised a procedure to estimate the surface dipole potential of Hg-supported SAMs.[10] The procedure consists in self-assembling the monolayers on a hanging mercury drop electrode and then measuring the charge involved during a progressive expansion of the mercury drop. This measurement is combined with an estimate of the charge density q experienced by diffuse layer ions, by measuring the diffuse layer capacitance of the SAM at different electrolyte concentrations by electrochemical impedance spectroscopy. We, therefore, found it interesting to apply this procedure to the estimate of the surface dipole potential of a number of Aib-based homo-oligopeptides thiolated at either the C- or N-terminus. As opposed to peptide systems based on coded α-amino acids, which start to form helices only for rather long oligomers,[11] Aib homopeptides have the peculiarity of forming stiff 3_{10}-helices even with a low number of monomeric units.[12−14] This is due to the marked steric hindrance of the α-carbon, which results in a restricted torsional freedom. Moreover, the increase in the number of units is accompanied by an increase in the number of intramolecular hydrogen bonds and a concomitant increase in stiffness. Studies

(8) (a) Morita, T.; Kimura, S. *J. Am. Chem. Soc.* **2003**, *125*, 8732–8733. (b) Watanabe, J.; Morita, T.; Kimura, S. *J. Phys. Chem. B* **2005**, *109*, 14416–14425. (c) Miura, Y.; Kimura, S.; Imanishi, Y.; Umemura, J. *Langmuir* **1998**, *14*, 6935–6940. (d) Kitagawa, K.; Morita, T.; Kimura, S. *Angew. Chem., Int. Ed.* **2005**, *44*, 6330–6333.

(9) (a) Mandal, H. S.; Kraaz, H.-B. *Chem. Phys.* **2006**, *326*, 246–251. (b) Wain, A. J.; Do, H. N. L.; Mandal, H. S.; Kraatz, H.-B.; Zhou, F. *J. Phys. Chem. C* **2008**, *112*, 14513–14519.

(10) Becucci, L.; Schwan, A. L.; Sheepwash, E. E.; Guidelli, R. *Langmuir* **2009**, *25*, 1828–1835.

(11) Goodman, M.; Toniolo, C.; Pallai, P. In *Forum Peptides*; Castro, B., Martinez, J., Eds.; Dhor: Nancy, France, 1985; pp 146−174.

(12) (a) Karle, I.; Balaram, P. *Biochemistry* **1990**, *29*, 6747–6756. (b) Toniolo, C.; Crisma, M.; Formaggio, F.; Peggion, C. *Biopolymers (Pept. Sci.)* **2001**, *60*, 396–419. (c) Toniolo, C.; Bonora, G. M.; Barone, V.; Bavoso, A.; Benedetti, E.; Di Blasio, B.; Grimaldi, P.; Lelj, F.; Pavone, V.; Pedone, C. *Macromolecules* **1985**, *18*, 895–902. (d) Toniolo, C.; Benedetti, E. *Trends Biochem. Sci.* **1991**, *16*, 350–353.

(13) (a) Polo, F.; Antonello, S.; Formaggio, F.; Toniolo, C.; Maran, F. *J. Am. Chem. Soc.* **2005**, *127*, 492–493. (b) Antonello, S.; Formaggio, F.; Moretto, A.; Toniolo, C.; Maran, F. *J. Am. Chem. Soc.* **2003**, *125*, 2874–2875.

(14) Fabris, L.; Antonello, S.; Armelao, L.; Donkers, R. L.; Polo, F.; Toniolo, C.; Maran, C. *J. Am. Chem. Soc.* **2006**, *128*, 326–336.

Chart 1. Peptides **3**+, **3**−, **5**+, and **5**− Highlighting Either the Different Polarity (**3**+ vs **3**−) or the Actual 3_{10}-Helix Structure (**5**+, **5**−)[a]

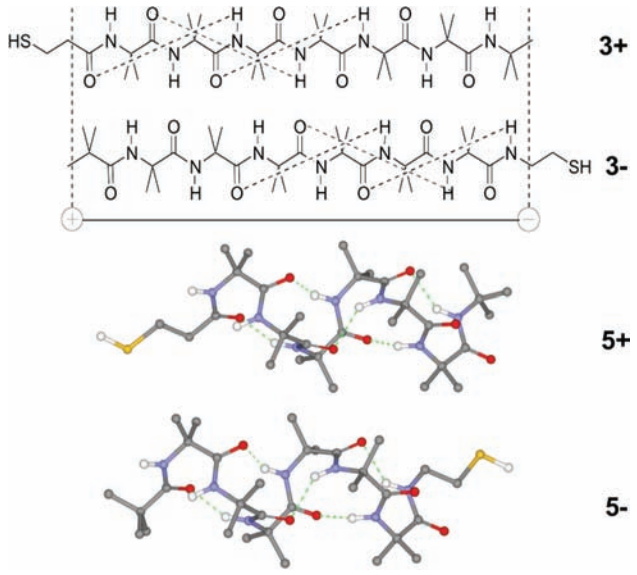

[a] The intramolecular C═O···H−N hydrogen bonds are denoted by dashed lines.

based on X-ray diffraction, IR, and ^{1}H NMR show that helical structures are formed in the solid state as well as in solution.[12c,15] The information so far gathered on this kind of peptides in other physical states indicates that the 3_{10}-helix structure is maintained unaltered also when the peptides are assembled onto gold surfaces. IRRAS evidence of it was reported for Aib homopeptides, thiolated on the N-terminus through a lipoic acid tether, in self-assembled monolayers on extended gold surfaces.[16] Analogously, we obtained IR and ^{1}H NMR spectroscopy results showing that the 3_{10}-helix conformation is maintained unaltered also when the same peptides decorate 1−2 nm gold clusters;[14] in this case, the peptides were thiolated on the N-terminus through a $-(CH_2)_2-$SH group. We also exploited the unique features of Aib homopeptides to promptly form stiff helices in order to introduce oriented dipoles into the capping monolayer of phenylethanethiolate-protected gold clusters.[17] Gradual exchange of the original ligands by Aib peptides thiolated at the N-terminus was found to cause a marked positive shift of the oxidation peaks of the gold core, thus pointing to very strong dipolar effects influencing the energy of the highest occupied molecular orbital of gold.

The peptides examined in the present work contain four or six Aib units. The molecular sequence is such as to allow the formation of structures characterized by three or five intramolecular C═O···H−N hydrogen bonds, as shown in Chart 1. The labeling **3**+, **3**−, **5**+, and **5**− denotes the number of such intramolecular hydrogen bonds and whether the N-terminus (+) or the C-terminus (−) is thiolated. The two couples of peptides **3**+/**3**− and **5**+/**5**− were devised in order to keep identical both their lengths and the nature of the group (*tert*-butyl) facing the solution.

Preliminary results on the experimental estimate of the dipole moments of a series of analogous Aib homo-oligomers in solution[18] show that the dipole moment increases linearly with the number of Aib units; accordingly, we estimate dipole moments of 11−12 and 16−17 D for the couples of peptides **3** and **5**, respectively. These data also show that 3_{10}-helices are far less sensitive to environment than α-helices, as also inferred from specific electrostatics calculations.[19] Despite the strong secondary structure of Aib peptides and the ensuing large values of the dipole moments, our electrochemical analysis indicates that a strong interfacial electric field between the mercury electrode and the electrolytic solution is capable of orienting the dipole moment of SAMs of Aib-peptides thiolated at the C-terminus against their "natural" molecular dipole moment.

2. Experimental Section

Chemicals. The water, obtained from an inverted osmosis unit, was distilled and then further distilled from alkaline permanganate. Merck Suprapur KCl was baked at 500 °C before use to remove any organic impurities. Tetramethyammonium chloride (TMACl) and hydroxide (TMAOH) were purchased from Merck and used as such. The following solvents, salts, and reagents were commercially available and used as received. Solvents: methanol, methylene chloride, diethyl ether, petroleum ether, ethyl acetate (Carlo Erba). Salts: potassium bisulfate, sodium bicarbonate, anhydrous sodium sulfate (Carlo Erba); *N*,*N*-diisopropylethylamine (DIEA), trifluoroacetic acid, triisopropylsilane, *tert*-butylamine, 2-aminoethanethiol (Acros Organics); triphenylmethanol, anhydrous acetonitrile, trimethylacetyl chloride (Sigma-Aldrich); 1-(3-dimethylaminopropyl)-3-ethylcarbodiimide hydrochloride (EDC·HCl), 1-hydroxy-7-aza-1,2,3-benzotriazole (HOAt) (GL Biochem, Shangai). The syntheses of $Ph_3C-S-(CH_2)_2-COOH$[20] and peptide **3**+[14] have been already described. The other thiolated Aib homopetides were prepared as follows.

***Z*-(Aib)$_6$−OH.** To a solution of *Z*-(Aib)$_6$−O*t*Bu (215 mg, 0.30 mmol) in 3 mL of anhydrous CH_2Cl_2 was added 3 mL of trifluoroacetic acid under stirring. After 1 h the solvent was evaporated and the remaining traces of trifluoroacetic acid were removed by repetitive evaporations with diethyl ether. The product was recrystallized from diethyl ether to give a colorless solid (yield 98%) having mp = 205−206 °C. IR (KBr): 3310, 1737,1704, 1659, 1530 cm^{-1}. ^{1}H NMR (400 MHz, $CDCl_3$): δ 1.37 (s, 6H, $2CH_3$), 1.42 (s, 6H, $2CH_3$), 1.45 (s, 6H, $2CH_3$), 1.47 (s, 16H, $4CH_3$), 1.51 (s, 6H, $2CH_3$), 5.10 (s, 2H, CH_2), 5.32, 6.29, 7.33 (3s, 3H, 3NH), 7.36 (m, 6H, 1NH, Ph), 7.38 (s, 1H, NH), 7.44 (s, 1H, NH).

***Z*-(Aib)$_6$−NH*t*Bu.** To an ice-cold solution of Z-(Aib)$_6$−OH (194 mg, 0.29 mmol) in 20 mL of anhydrous acetonitrile was added EDC·HCl (58 mg, 0.30 mmol), followed after 1 h by addition of *tert*-buthylamine (315 μL, 3.00 mmol). The reaction mixture was stirred 3 days at room temperature and then evaporated to dryness. The crude product was purified by column chromatography using as the eluent petroleum ether/ethyl acetate (v/v 1/1, 1/2, 1/3, 1/4) and recrystallized from ethyl acetate/petroleum ether to give *Z*-(Aib)$_6$−NH*t*Bu as a colorless solid (yield = 70%) having mp = 219−221 °C. IR (KBr): 3428, 3321, 2985, 2940, 1703, 1663, 1530, 1454 cm^{-1}. ^{1}H NMR ($CDCl_3$): δ 1.31 (s, 6H, $2CH_3$), 1.39 (s, 9H, *t*Bu), 1.43 (s, 6H, $2CH_3$), 1.48 (s, 18H, $6CH_3$), 1.51 (s, 6H, $2CH_3$), 5.11 (s, 2H, CH_2), 5.89, 6.49, 6.89 (3s, 3H, 3NH), 7.36 (m, 6H, 1NH, Ph), 7.50 (s, 2H, 2NH), 7.56 (s, 1H, NH).

$Ph_3C-S-(CH_2)_2-CO-$(Aib)$_6$−NH*t*Bu. To an ice-cold solution of $Ph_3C-S-(CH_2)_2-$COOH (150 mg, 0.43 mmol) in 10 mL of anhydrous CH_2Cl_2 were added HOAt (60 mg, 0.44 mmol) and

(15) (a) Kennedy, D. F.; Crisma, M.; Toniolo, C.; Chapman, D. *Biochemistry* **1991**, *30*, 6541. (b) Hanson, P.; Millhauser, F.; Formaggio, F.; Crisma, M.; Toniolo, C. *J. Am. Chem. Soc.* **1996**, *118*, 7618.
(16) Wen, X.; Linton, R. W.; Formaggio, F.; Toniolo, C.; Samulski, E. T. *J. Phys. Chem. A* **2004**, *108*, 9673–9681.
(17) Holm, A. H.; Ceccato, M.; Donkers, R. L.; Fabris, L.; Pace, G.; Maran, F. *Langmuir* **2006**, *22*, 10584–10589.
(18) Di Noto, V.; Maran, F., work in progress.
(19) Sengupta, D.; Behera, R. N.; Smith, J. C.; Ullmann, G. M. *Structure* **2005**, *13*, 849–855.
(20) Peggion, C.; Formaggio, F.; Toniolo, C.; Becucci, L.; Moncelli, M. R.; Guidelli, R. *Langmuir* **2001**, *17*, 6585–6592.

EDC·HCl (85 mg, 0.44 mmol), followed by addition of a solution of H−(Aib)$_6$−NH*t*Bu (obtained, and used as such, by catalytic hydrogenation of 200 mg, 0.28 mmol, of Z-(Aib)$_6$−NH*t*Bu in MeOH) in anhydrous CH_2Cl_2 containing DIEA (50 μL, 0.28 mmol). After stirring for 48 h at room temperature, the reaction mixture was evaporated to dryness. The crude product was purified by column chromatography using as the eluent petroleum ether/ethyl acetate (v/v 1/2, 1/3, 1/4, 1/5) and recrystallized from ethyl acetate/petroleum ether to give $Ph_3C-S-(CH_2)_2-$ CO−(Aib)$_6$−NH*t*Bu as a colorless solid (yield = 67%) having mp = 251−253 °C. IR (KBr): 3420, 3308, 2985, 2932, 1660, 1533 cm^{-1}. ^{1}H NMR (CD_3CN): δ 1.28 (s, 6H, 2CH$_3$), 1.32 (s, 9H, *t*Bu), 1.35 (s, 6H, 2CH$_3$), 1.35 (s, 6H, 2CH$_3$), 1.38 (s, 6H, 2CH$_3$), 1.40 (s, 12H, 4CH$_3$), 2.22 (t, 2H, CH_2), 2.42 (t, 2H, CH_2), 6.82, 6.90, 6.94 (3s, 3H, 3NH), 7.24−7.44 (m, 16H, 1NH, 3Ph), 7.58, 7.62, 7.68 (3s, 3H, 3NH).

HS−(CH$_2$)$_2$−CO−(Aib)$_6$−NH*t*Bu (5+). $Ph_3C-S-(CH_2)_2$ −CO−(Aib)$_6$−NH*t*Bu (56 mg, 0.06 mmol) was dissolved in 10 mL of a 7/2/1 mixture of CH_2Cl_2/trifluoroacetic acid/triisopropylsilane. After stirring for 1 h at room temperature, the solvent was evaporated and the remaining traces of trifluoroacetic acid were removed by repetitive evaporations with diethyl ether. The crude product was purified by column chromatography using the eluent CH_2Cl_2 and then CH_2Cl_2/EtOH, 10/1. After crystallization from diethyl ether HS−(CH$_2$)$_2$−CO−(Aib)$_6$−NH*t*Bu was obtained as a colorless solid (yield 68%) having mp = 270−271 °C. IR (KBr): 3424, 3313, 3049, 2985, 2934, 2872, 1662, 1539 1455 cm^{-1}. ^{1}H NMR ($CDCl_3$): δ 1.40 (s, 9H, *t*Bu), 1.42−1.58 (m, 36H, 12CH$_3$), 2.64 (t, 2H, CH_2-CO), 2.86 (m, 2H, S−CH_2), 6.83, 6.89, 7.51, 7.60, 7.66, 7.75, 7.78 (7s, 7H, 7NH). ESI-TOF: $[M + H]^+_{calc}$ = 672.9; $[M + H]^+_{exp}$ = 672.3.

C(CH$_3$)$_3$−CO−(Aib)$_2$−O*t*Bu. To a solution of H−(Aib)$_2$−O*t*Bu (obtained, and used as such, by catalytic hydrogenation of 200 mg, 0.53 mmol, of Z-(Aib)$_2$−O*t*Bu in MeOH) in 20 mL of anhydrous CH_2Cl_2 were added C(CH$_3$)$_3$−CO−Cl (100 μL, 0.81 mmol) and DIEA (140 μL, 0.81 mmol). After stirring for 3 days at room temperature, the reaction mixture was evaporated to dryness. The crude product was purified by column chromatography using, as the eluent, petroleum ether/ethyl acetate (v/v 3/1) and recrystallized from ethyl acetate/petroleum ether to give C(CH$_3$)$_3$−CO−(Aib)$_2$−O*t*Bu as a colorless solid (yield = 90%) having mp = 139−140 °C. IR (KBr): 3392, 3352, 2978, 2964, 2937, 1721, 1675, 1654, 1523 cm^{-1}. ^{1}H NMR ($CDCl_3$) δ 1.20 (s, 9H, *t*Bu), 1.46 (s, 9H, *t*Bu), 1.53 (s, 6H, 2CH$_3$), 1.57 (s, 6H, 2CH$_3$), 6.47 (s, 1H, NH), 7.03 (s, 1H, NH).

C(CH$_3$)$_3$−CO−(Aib)$_4$−O*t*Bu. To a solution of H−(Aib)$_4$−O*t*Bu (obtained, and used as such, by catalytic hydrogenation of 2.00 g, 3.65 mmol, of *Z*-(Aib)$_4$−O*t*Bu in MeOH) in 20 mL of anhydrous CH_2Cl_2 were added C(CH$_3$)$_3$−CO−Cl (0.47 mL, 3.80 mmol) and DIEA (1.2 mL, 7.20 mmol). After stirring for 3 days at room temperature the reaction mixture was treated as described above for *Z*-(Aib)$_2$−O*t*Bu to give C(CH$_3$)$_3$−CO−(Aib)$_4$−O*t*Bu as a colorless solid (yield = 65%) having mp = 198−199 °C. IR: 3435, 3417, 3346, 2983, 2936, 2872, 1734, 1663, 1619, 1457 (KBr) cm^{-1}. ^{1}H NMR ($CDCl_3$): δ 1.20 (s, 9H, *t*Bu), 1.39 (s, 6H, 2CH$_3$), 1.40 (s, 9H, *t*Bu), 1.44 (s, 6H, 2CH$_3$), 1.45 (s, 6H, 2CH$_3$), 1.49 (s, 6H, 2CH$_3$), 5.93, 6.12, 7.19, 7.24 (4s, 4H, 4NH).

C(CH$_3$)$_3$−CO−(Aib)$_2$−OH. To a solution of C(CH$_3$)$_3$ −CO−(Aib)$_2$−O*t*Bu (150 mg, 0.46 mmol) in 3 mL of anhydrous CH_2Cl_2 was added 3 mL of trifluoroacetic acid under stirring. After 1 h the solvent was evaporated and the remaining traces of trifluoroacetic acid were removed by repetitive evaporations with diethyl ether. The product was recrystallized from diethyl ether to give a colorless solid (yield = 90%) having mp = 189−190 °C. IR (KBr): 3394, 3375, 3320, 3300, 2989, 2940, 2875, 1725, 1667, 1623, 1517 cm^{-1}. ^{1}H NMR ($CDCl_3$): δ 1.21 (s, 9H, *t*Bu), 1.53 (s, 6H, 2CH$_3$), 1.56 (s, 6H, 2CH$_3$), 6.16 (s, 1H, NH), 7.61 (s, 1H, NH).

C(CH$_3$)$_3$−CO−(Aib)$_6$−O*t*Bu. To an ice-cold solution of C(CH$_3$)$_3$−CO−(Aib)$_2$−OH (125 mg, 0.46 mmol) in 10 mL of anhydrous acetonitrile was added EDC·HCl (105 mg, 0.55 mmol), followed by addition of a solution of H−(Aib)$_4$−NH*t*Bu (obtained, and used as such, by catalytic hydrogenation of 300 mg, 0.55 mmol, of *Z*-(Aib)$_4$−NH*t*Bu in MeOH) in 20 mL of anhydrous acetonitrile. After heating at 80 °C for 3 days the reaction was evaporated to dryness. The crude product was purified by column chromatography using as the eluent petroleum ether/ethyl acetate (v/v 1/3) and recrystallized from ethyl acetate/petroleum ether to give a colorless solid (yield = 43%) having mp = 217−218 °C. IR (KBr): 3427, 3293, 2985, 2937, 2871, 1744, 1698, 1656, 1531, 1456 cm^{-1}. ^{1}H NMR ($CDCl_3$): δ 1.24 (s, 9H, *t*Bu), 1.42−1.58 (m, 45H, 9H *t*Bu, 12CH$_3$), 6.09, 6.15, 7.30, 7.39, 7.52, 7.63 (6s, 6H, 6NH).

C(CH$_3$)$_3$−CO−(Aib)$_4$−OH. To a solution of C(CH$_3$)$_3$ −CO−(Aib)$_4$−O*t*Bu (1.00 g, 2.01 mmol) in 3 mL of anhydrous CH_2Cl_2 was added 3 mL of trifluoroacetic acid under stirring. After 1 h the solvent was evaporated and the remaining traces of trifluoroacetic acid were removed by repetitive evaporations with diethyl ether. The product was recrystallized from diethyl ether to give a colorless solid (yield = 80%) having mp = 228−229 °C. IR (KBr): 3422, 3356, 3327, 3294, 3177, 2986, 2938, 1747, 1673, 1646, 1528 cm^{-1}. ^{1}H NMR ($CDCl_3$): δ 1.13 (s, 9H, *t*Bu), 1.24 (s, 6H, 2CH$_3$), 1.32 (s, 18H, 6CH$_3$), 7.35, 7.38, 7.50, 7.64 (4s, 4H, 4NH).

C(CH$_3$)$_3$−CO−(Aib)$_6$−OH. To a solution of C(CH$_3$)$_3$ −CO−(Aib)$_6$−O*t*Bu (130 mg, 0.19 mmol) in 3 mL of anhydrous CH_2Cl_2 was added 3 mL of trifluoroacetic acid under stirring. After 1 h the solvent was evaporated and the remaining traces of trifluoroacetic acid were removed by repetitive evaporations with diethyl ether. The product was recrystallized from diethyl ether to give a colorless solid (yield = 80%) having mp = 285−286 °C. IR (KBr): 3418, 3293, 2986, 2940, 2872, 1740, 1657, 1532, 1456 cm^{-1}. ^{1}H NMR ($CDCl_3$): δ 1.22 (s, 9H, *t*Bu), 1.42−1.55 (m, 36H, 12CH$_3$), 7.28, 7.32, 7.40, 7.55, 7.58, 7.66 (6s, 6H, 6NH).

(Ph)$_3$C−S−CH$_2$CH$_2$−NH$_2$·H$_2$SO$_4$. To an ice-cold solution of HS−CH_2CH_2−NH_2·HCl (0.26 g, 2.29 mmol) and $(Ph)_3C-OH$ (1.00 g, 3.84 mmol) in 40 mL of acetic acid was added dropwise H_2SO_4(conc) until the yellow color remained persistent. After 30 min the reaction mixture was concentrated to 10 mL, and 150 mL of diethyl ether was added. The white precipitate was filtered and washed several times with diethyl ether. Yield = 80%. Mp = 194−195 °C. IR (KBr): 3428, 3052, 2928, 1636, 1513, 1488, 1444, 1221, 1180, 1162, 1061, 1017 cm^{-1}. ^{1}H NMR (DMSO-d_6): δ 2.43 (m, 2H, CH_2), 2.51 (m, 2H, CH_2), 7.21−7.41 (m, 15H, 3Ph), 7.66 (s, 2H, NH_2).

C(CH$_3$)$_3$−CO−(Aib)$_4$−NH−(CH$_2$)$_2$−S−C(Ph)$_3$. To an ice-cold solution of C(CH$_3$)$_3$−CO−(Aib)$_4$−OH (1.50 g, 3.39 mmol) in 20 mL of anhydrous CH_2Cl_2 was added EDC·HCl (0.65 g, 3.39 mmol), followed after 1 h by addition of $(Ph)_3C-S-CH_2CH_2-NH_2\cdot H_2SO_4$ (2.83 g, 6.78 mmol) and DIEA (1.16 mL, 6.78 mmol). The reaction mixture was stirred for 3 days at room temperature and evaporated to dryness. The oily residue was dissolved in ethyl acetate, and the organic solution was washed with 10% $KHSO_4$, H_2O, 5% $NaHCO_3$, and H_2O. The organic layer was dried over anhydrous Na_2SO_4 and evaporated to dryness. The product was recrystallized from ethyl acetate/petroleum ether to give C(CH$_3$)$_3$− CO−(Aib)$_4$ −NH−(CH$_2$)$_2$−S−C(Ph)$_3$ as a colorless solid (yield = 61%) having mp = 245−247 °C. IR (KBr): 3433, 3317, 1660, 1530, 741, 699 cm^{-1}. ^{1}H NMR (DMSO-d_6): δ 1.13 (s, 9H, *t*Bu), 1.19 (s, 6H, 2CH$_3$), 1.27 (s, 6H, 2CH$_3$), 1.30 (s, 6H, 2CH$_3$), 1.32 (s, 6H, 2CH$_3$), 2.20 (t, 2H, β-CH_2), 2.90 (m, 2H, α-CH_2), 7.20−7.31 (m, 17H, 2NH, 3Ph), 7.55 (s, 1H, NH), 7.63 (s, 1H, NH), 7.78 (s, 1H, NH).

C(CH$_3$)$_3$−CO−(Aib)$_6$−NH−(CH$_2$)$_2$−S−C(Ph)$_3$. To an ice-cold solution of C(CH$_3$)$_3$−CO−(Aib)$_6$−OH (119 mg, 0.19 mmol) in 20 mL of anhydrous acetonitrile was added EDC·HCl (45 mg, 0.23 mmol), followed after 1 h by addition of $(Ph)_3C-S-CH_2CH_2$ $-NH_2\cdot H_2SO_4$ (162 mg, 0.39 mmol) and DIEA (67 μL, 0.39 mmol). The reaction mixture was stirred for 4 days at room temperature and evaporated to dryness. The crude product was purified by column chromatography using as the eluent petroleum ether/ethyl acetate (v/v 1/2, 1/3, 1/4, 1/5) and recrystallized from ethyl acetate/

petroleum ether to give a colorless solid (yield = 68%) having mp = 259−260 °C. IR (KBr): 3358, 3057, 2964, 2932, 2244, 1658, 1504 cm^{-1}. ^1H NMR ($CDCl_3$): δ 1.24 (s, 9H, *t*Bu), 1.38 (s, 6H, $2CH_3$), 1.42 (s, 6H, $2CH_3$), 1.47 (m, 18H, $3CH_3$), 1.52 (s, 6H, $2CH_3$), 2.40 (t, 2H, β-CH_2), 3.19 (m, 2H, α-CH_2), 6.03 (s, 1H, NH), 6.13 (s, 1H, NH), 7.08−7.42 (m, 17H, 2NH, 3Ph), 7.50 (s, 1H, NH), 7.55 (s, 1H, NH), 7.66 (s, 1H, NH).

$C(CH_3)_3$−CO−$(Aib)_4$−NH−$(CH_2)_2$−SH (3−). $C(CH_3)_3$−CO−$(Aib)_4$−NH−$(CH_2)_2$−S−Trt (1.50 g, 2.02 mmol) was dissolved in 20 mL of a 7/2/1 mixture of CH_2Cl_2/trifluoroacetic acid/triisopropylsilane. The solution was stirred for 2 h at room temperature, and then the solvent was evaporated. The crude product was washed with diethyl ether to remove the traces of trifluoroacetic acid by evaporation. After crystallization from diethyl ether $C(CH_3)_3$−CO−$(Aib)_4$−NH−$(CH_2)_2$−SH was obtained as a colorless solid (yield 83%). IR (KBr): 3416, 3313, 2524, 1665, 1642, 1536 cm^{-1}. ^1H NMR ($CDCl_3$): δ 1.24 (s, 9H, *t*Bu), 1.42 (s, 6H, $2CH_3$), 1.47 (s, 6H, $2CH_3$), 1.49 (s, 6H, $2CH_3$), 1.54 (s, 6H, $2CH_3$), 1.78 (t, 1H, SH), 2.71 (t, 2H, β-CH_2), 2.46 (m, 2H, α-CH_2), 5.93 (s, 1H, NH), 6.08 (s, 1H, NH), 7.24 (s, 1H, NH), 7.53 (t, 1H, NH), 7.63 (s, 1H, NH). ESI-TOF: $[M + H]^+_{calc} = 502.7$; $[M + H]^+_{exp} = 502.4$.

$C(CH_3)_3$−CO−$(Aib)_6$−NH−$(CH_2)_2$−SH (5−). $C(CH_3)_3$ −CO−Aib_6−NH−$(CH_2)_2$−S−Trt (60 mg, 0.0656 mmol) was dissolved in 10 mL of a 7/2/1 mixture of CH_2Cl_2/trifluoroacetic acid/triisopropylsilane. The solution was stirred for 1 h at room temperature, and then the solvent was evaporated. The crude product was washed with diethyl ether to remove the traces of trifluoroacetic acid by evaporation and purified by column chromatography using the eluent CH_2Cl_2 and then CH_2Cl_2/EtOH, 10/1. After crystallization from diethyl ether $C(CH_3)_3$−CO−$(Aib)_6$−NH−$(CH_2)_2$−SH was obtained as a colorless solid (yield 85%) having mp = 262−264 °C. IR (KBr): 3432, 3301, 2984, 2937, 1657, 1531 cm^{-1}. ^1H NMR ($CDCl_3$): δ 1.24 (s, 9H, *t*Bu), 1.42 (s, 6H, $2CH_3$), 1.48 (s, 24H, $8CH_3$), 1.56 (s, 6H, $2CH_3$), 1.81 (t, 1H, SH), 2.70 (m, 2H, CH_2), 3.46 (m, 2H, CH_2), 6.19 (s, 1H, NH), 6.21 (s, 1H, NH), 7.40 (s, 1H, NH), 7.60 (s, 1H, NH), 7.63 (m, 1H, NH), 7.71 (s, 1H, NH). ESI-TOF: $[M + H]^+_{calc} = 672.9$; $[M + H]^+_{exp} = 672.4$.

Electrochemical Apparatus and Methodologies. All measurements were carried out in aqueous solutions of KCl or TMACl. Use was made of a homemade hanging mercury drop electrode (HMDE), described elsewhere.[21] A homemade glass capillary with a finely tapered tip, about 1 mm in outer diameter, was employed. Capillary and mercury reservoir were thermostated at 25 ± 0.1 °C in a water-jacketed box to avoid any changes in drop area due to a change in temperature. Chronocoulometric, cyclic voltammetric, and electrochemical impedance spectroscopy measurements were carried out with an Autolab PGSTAT 12 instrument (Echo Chemie, Utrecht, The Netherlands) supplied with an FRA2 module for impedance measurements, SCAN-GEN scan generator, and GPES 4.9005 Beta software. Potentials were measured vs a Ag|AgCl electrode immersed in the KCl or TMACl working solution and are referred to a Ag|AgCl|0.1 M KCl reference electrode.

The self-assembly of the thiolated-peptide monolayers on the HMDE was carried out by keeping the mercury drop immersed in ethanol solutions of the thiolated peptides for about 90 min. The peptide-coated mercury electrode was stabilized by scanning the applied potential several times over the appropriate potential range (see further, inset of Figure 1) and by recording the differential capacitance *C*, measured at 75 Hz upon simulating the SAM by a resistance and a capacitance in parallel.

A SAM-coated mercury drop can often be expanded to a large extent without causing the SAM to collapse. This situation is encountered with SAMs of phospholipids,[22] *n*-alkanethiols with chain lengths less than 14,[23] and thiolipids.[20,24] In this case, the amount of SAM material on the drop surface remains constant

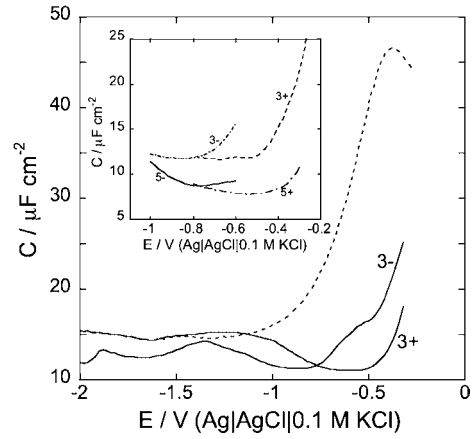

Figure 1. Curves of the differential capacitance *C* against the applied potential *E* for Hg-supported **3**+ and **3**− SAMs in aqueous 0.1 M TMACl, obtained at 75 Hz upon simulating the SAMs by a resistance and a capacitance in parallel. The dashed curve is the differential capacitance curve for bare mercury in the same medium. The inset shows *C* vs *E* curves for Hg-supported **3**+, **3**−, **5**+, and **5**− SAMs in aqueous 0.1 M KCl over the potential ranges in which the SAMs were stabilized.

during the drop expansion, while the self-assembled molecules undergo a progressive tilt without incorporating water molecules. Denoting by θ the tilt angle of the self-assembled molecules with respect to the monolayer normal, the monolayer thickness, $d(\theta)$, at a given stage of the expansion is given by $d \cos \theta$. Incidentally, the quantities whose dependence upon θ is not explicitly expressed refer to the initial unexpanded drop. The expansion of the drop area, $A(\theta)$, does not alter the monolayer volume, $A(\theta) \times d(\theta) = A \times d$; consequently, $A(\theta)$ is equal to $A/\cos \theta$. An accurate measurement of the volume of the spherical mercury drop progressively extruded from the capillary of the HMDE allows $\cos \theta$ to be estimated from the $A/A(\theta)$ ratio. The constancy of the number of SAM molecules during the drop expansion causes their number density *N* to decrease according to the relationship $N(\theta) = NA/A(\theta) = N \cos \theta$. The dipole moment normal component, μ, of the molecules of the unexpanded SAM, if any, undergoes the same tilt as *d* during the drop expansion, thus causing it to vary according to the relationship $\mu(\theta) = \mu \cos \theta$. The above approximate assumptions exclude the possibility that the drop expansion may cause the formation of thiol-free and thiol-covered areas, which would result in an abrupt increase in capacitance. Such an abrupt increase in capacitance, indicative of monolayer breakdown, was reported, for instance, with mercury-supported monolayers of *n*-alkanethiols with more than 14 carbon atoms.[23a,b] No such behavior was observed with the present peptides, as their capacitance increased smoothly with drop expansion.

The rationale behind the procedure for measuring the surface dipole potential of Hg-supported SAMs is described in detail elsewhere.[10] Suffice it here to say that the opposite of the surface dipole potential produced by the dipole moment of the SAM molecules, $\chi = N\mu/(\nabla\nabla_0)$, where ∇_0 is the permittivity of free space, is given by the slope of the quantity

$$\xi(\theta) \equiv \{q(\theta) \cos \theta / C_{SAM} + \psi[c, q(\theta)]\} \qquad (1)$$

against $\cos^2 \theta$, at constant applied potential, *E*. Here, $q(\theta)$ is the charge density experienced by the diffuse layer ions, C_{SAM} is the

(21) Moncelli, M. R.; Becucci, L. *J. Electroanal. Chem.* **1997**, *433*, 91–96.

(22) Becucci, L.; Moncelli, M. R.; Herrero, R.; Guidelli, R. *Langmuir* **2000**, *16*, 7694–7700.

(23) (a) Slowinski, K.; Chamberlain, R. V.; Miller, C. J.; Majda, M. *J. Am. Chem. Soc.* **1997**, *119*, 11910–11919. (b) Bruckner-Lea, C.; Kimmel, R. J.; Janata, J.; Conroy, J. F. T.; Caldwell, K. *Electrochim. Acta* **1995**, *40*, 2897–2904.

(24) Becucci, L.; Guidelli, R.; Liu, Q.; Bushby, R. J.; Evans, S. D. *J. Phys. Chem. B* **2002**, *106*, 10410–10416.

differential capacitance of the unexpanded SAM, and $\psi[c,q(\theta)]$ is the potential difference across the diffuse layer adjacent to the SAM, regarded as a function of the electrolyte concentration c and of the charge density $q(\theta)$.

The only thermodynamically significant charge density on a metal surface is the "total charge density" $\sigma_M(E)$, namely, the charge density to be supplied to the electrode to keep the applied potential E constant when the electrode surface is increased by unity, and the composition of the electrified interface maintains its equilibrium value during such an increase. It is obtained by starting with an uncoated electrode immersed in a solution of the supporting electrolyte alone and stepping the applied potential from the potential of zero charge (pzc) to a final potential E_f negative enough to exclude adsorption of the adsorbate under investigation, provided such a potential is experimentally accessible: the charge accompanying the potential step pzc $\rightarrow E_f$ is just the common value, $\sigma_M(E_f)$, of the total charge density both in the presence and in the absence of the adsorbate. The charge accompanying a further potential step from any given initial potential E to E_f at a SAM-coated electrode in the same supporting electrolyte is equal to $\sigma_M(E_f) - \sigma_M(E)$, thus allowing the estimate of the total charge density $\sigma_M(E)$ at E.

The total charge density σ_M coincides with that, q, experienced by the diffuse layer ions only when the self-assembling surfactant molecules are neutral and do not generate a charge in direct contact with the electrode surface during their self-assembly. Usually, this requirement is not fulfilled by molecules terminated with a sulfhydryl group. In fact, during the self-assembly, sulfhydryl groups may undergo deprotonation. In this case a negative charge is formed in direct contact with the electrode surface, independent of whether it may be partially or totally transferred to the electrode. The diffuse layer ions will then experience both σ_M and this additional negative charge. In this case, the total charge density σ_M at a potential E at which the SAM is stable, measured by stepping the potential from E to a potential E_f at which it is desorbed, is positive and relatively high[25] to maintain the applied potential E constant in spite of the negative charge due to the SAM molecules. It is evident that it is q, rather than σ_M, which generates the potential drop across the SAM, once divided by the differential capacitance C_{SAM} of the monolayer. However, as opposed to σ_M, q can only be estimated on the basis of extrathermodynamic assumptions.

A convenient way to estimate q is based on the use of Gouy−Chapman theory for the diffuse layer. According to this approximate theory, the differential capacitance, C_d, of the diffuse layer depends exclusively upon q and the bulk concentration, c, of the electrolyte. Thus, C_d^{-1} values, calculated at different electrolyte concentrations c and at constant q on the basis of the Gouy−Chapman theory, can be plotted against the corresponding values calculated for zero q, $C_d(q = 0)^{-1}$, yielding a series of calculated C_d^{-1} vs $C_d(q = 0)^{-1}$ curves at different q values.[10] Plotting experimental C_d^{-1} values, measured at different electrolyte concentrations c, against the $C_d(q = 0)^{-1}$ values calculated for the same electrolyte concentrations and comparing the resulting plot with the series of calculated C_d^{-1} vs $C_d(q = 0)^{-1}$ plots allows the q value providing the best fit to be sorted out.

The expansion of a mercury drop coated with a SAM that does not collapse is accompanied by the flow of a charge $Q(\theta)$ that consists in an increment of q rather than of σ_M. In fact, the number of SAM molecules anchored to the electrode is unchanged during the expansion, and the same is true for any charge that they keep in contact with the electrode surface. Hence, to maintain the applied potential constant, the charge $Q(\theta)$ that reaches the metal surface along the external circuit during the drop expansion causes exclusively a change in the diffuse layer charge. The charge density $q(\theta)$ to be used in eq 1 is obtained by adding the charge $Q(\theta)$ following the drop expansion to the charge Aq on the initial unexpanded drop, as estimated from a C_d^{-1} vs $C_d(q = 0)^{-1}$ plot, and dividing this sum by $A(\theta)$:

$$q(\theta) = [Q(\theta) + Aq]/A(\theta) \quad (2)$$

3. Results

Differential Capacitance of the Peptide SAMs by ac Voltammetry at 75 Hz. To verify the possible reductive desorption of the Aib-peptide SAMs at sufficiently negative potentials, their differential capacitance C was measured over the potential range from −0.20 to −2.15 V in aqueous TMACl. In fact, the double-layer region on bare mercury in this electrolyte extends up to −2.15 V before the onset of hydrogen evolution.[26] Figure 1 shows the C vs E curves of **3**+ and **3**− SAMs in 0.1 M TMACl at 75 Hz upon simulating the SAMs by a resistance and a capacitance in parallel.

The differential capacitance curve of the **3**+ SAM merges with that of bare mercury at potentials negative of −1.60 V, thus suggesting complete peptide desorption at these potentials. However, no pseudocapacitance desorption peak is observed. Conversely, the differential capacitance curve of the **3**− SAM is lower than that of bare mercury at all accessible potentials. The differential capacitance curves of the **5**+ and **5**− SAMs are very close to those of the **3**+ and **3**− SAMs, respectively. The mode of desorption of **3**+ and **5**+ is thus different from that of **3**− and **5**−, as will be argued in connection with chronocoulometric measurements.

The inset of Figure 1 shows plots of the differential capacitance curves of Hg-supported SAMs of **3**− and **5**− from −0.60 to −1.0 V, and of **3**+ and **5**+ from −0.30 to −0.80 V, in aqueous 0.1 M KCl. The curves were obtained after stabilizing the SAMs by means of repeated potential scans over the corresponding potential ranges. These potential ranges were chosen because the SAMs were found to be stable in time and reproducible therein, thus allowing accurate measurements of the diffuse layer capacitance by electrochemical impedance spectroscopy (EIS).

Differential Capacitance of the Peptide SAMs by Impedance Spectroscopy. The diffuse layer capacitance of the four Hg-supported thiopeptide SAMs in contact with KCl aqueous solutions of different concentrations was estimated from their impedance spectra at constant applied potential E. The Aib-peptide SAMs were found to be particularly stable in time at potentials corresponding to the flat minimum of the corresponding differential capacitance curves in the inset of Figure 1. Thus, the **3**+, **5**+, and **5**− SAMs were investigated at −0.75 V, whereas the **3**− SAM was investigated at −0.95 V. The impedance spectra were fitted to an equivalent circuit consisting of four *RC* meshes in series. These meshes simulate four different dielectric slabs, namely, the sulfide ion bound to the mercury surface, the peptide chain, the diffuse layer, and the aqueous solution adjacent to the SAM. Typical values of the resistance and capacitance of the **5**+ and **5**− peptide chains in 0.1 M KCl are 1 MΩ cm^2 and 10 μF cm^{-2}; those of the **3**+ and **3**− peptide chains are 0.9 MΩ cm^2 and 13 μF cm^{-2}. The resistance and capacitance values ascribed to the sulfide ion bound to mercury are on the order of 10 kΩ cm^2 and 50 μF cm^{-2}.

(25) (a) Widrig, C. A.; Chung, C.; Porter, M. D. *J. Electroanal. Chem.* **1991**, *310*, 335–359. (b) Schneider, T. W.; Buttry, D. A. *J. Am. Chem. Soc.* **1993**, *115*, 12391–12397. (c) Yang, D. F.; Wilde, C. P.; Morin, M. *Langmuir* **1996**, *12*, 6570–6577; **1997**, *13*, 243−248. (d) Kakiuchi, T.; Usui, H.; Hobara, D.; Yamamoto, M. *Langmuir* **2002**, *18*, 5231–5238. (e) Laredo, T.; Leitch, J.; Chen, M.; Burgess, I. J.; Dutcher, J. R.; Lipkowski, J. *Langmuir* **2007**, *23*, 6205–6211.

(26) Tadini Buoninsegni, F.; Becucci, L.; Moncelli, M. R.; Guidelli, R. *J. Electroanal. Chem.* **2001**, *500*, 395–407.

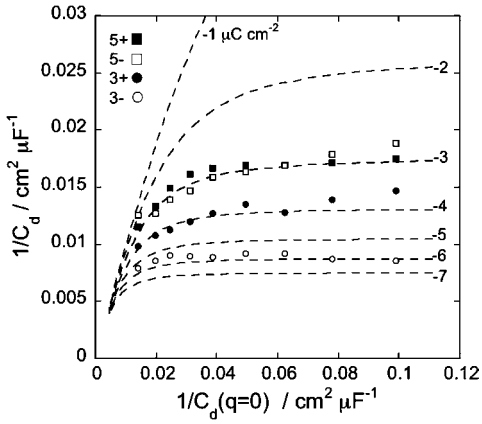

Figure 2. Dashed curves are $1/C_d$ vs $1/C_d(q = 0)$ plots calculated from the Gouy−Chapman theory for the q values reported on each curve. The solid squares, open squares, solid circles, and open circles are experimental values of $1/C_d$ against the corresponding $1/C_d(q = 0)$ values for Hg-supported SAMs of **5**+, **5**−, **3**+, and **3**−, respectively, in aqueous KCl of concentration 0.1, 5×10^{-2}, 3.2×10^{-2}, 2×10^{-2}, 1.3×10^{-2}, 8×10^{-3}, 5×10^{-3}, 3.2×10^{-3}, and 2×10^{-3} M (from left to right). Measurements were carried out at −0.75 V for the **5**+, **5**−, and **3**+ SAMs and at −0.95 V for the **3**− SAM.

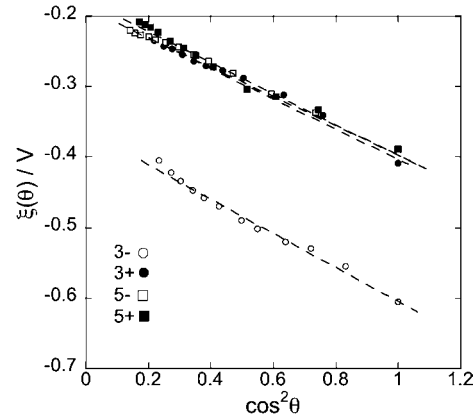

Figure 3. Plots of $\xi(\theta)$ vs $\cos^2\theta$ for Hg-supported SAMs of **3**− (open cirles), **3**+ (solid circles), **5**− (open squares), and **5**+ (solid squares) in aqueous 0.1 M KCl. The plots refer to −0.75 V for the **5**+, **5**−, and **3**+ SAMs and to −0.95 V for the **3**− SAM.

The reciprocal of the diffuse layer capacitance C_d, estimated at different KCl concentrations by the above procedure, is plotted against the corresponding calculated $C_d(q = 0)^{-1}$ value in Figure 2. Note that the increase in KCl concentration at constant applied potential compresses the ionic atmosphere, thus increasing the diffuse layer capacitance, C_d. The experimental points in Figure 2 correspond to progressively increasing KCl concentrations as one proceeds from right to left. Consequently, C_d increases in the same direction and its reciprocal decreases, in accordance with the Gouy−Chapman theory. The best agreement between the four experimental C_d^{-1} vs $C_d(q = 0)^{-1}$ plots and the dashed curves calculated for different q values is obtained with $q(-0.75\ \text{V}) = -3\ \mu\text{F cm}^{-2}$ for the **5**+ and **5**− SAMs, with $q(-0.75\ \text{V}) = -4\ \mu\text{F cm}^{-2}$ for the **3**+ SAM, and with $q(-0.95\ \text{V}) = -6\ \mu\text{F cm}^{-2}$ for the **3**− SAM. The more negative q value for the latter SAM is simply due to the more negative potential at which it was measured. The difference between the $q(-0.95\ \text{V})$ value for the **3**− SAM and the $q(-0.75$ V) value for the **3**+ SAM is compatible with the differential capacitance C_{SAM} of the peptide chains of the **3**+ and **3**− SAMs, which was found to be equal to $\sim 11\ \mu\text{F cm}^{-2}$ from ac voltammetric measurements. Analogous measurements on the **5**+ and **5**− SAMs yield a C_{SAM} value of $\sim 8.5\ \mu\text{F cm}^{-2}$.

Estimate of the Surface Dipole Potential of the Peptide SAMs. After determining the charge density q on the Hg-supported Aib-peptide SAMs experienced by the diffuse layer ions, the final step for the estimate of the surface dipole potential of these SAMs consists in measuring the change of q with increasing the drop size. The charge $Q(\theta)$ following the progressive expansion of the SAM-coated mercury drop was obtained by extruding mercury gradually from the capillary by manual advancement of the piston of the mercury reservoir and by recording the charge increment, ΔQ, flowing as a consequence of each piston advancement. Adding the charge increment involved in each piston advancement to the sum of all preceding charge increments yields the charge $Q(\theta)$. Inserting $Q(\theta)$ in eq 2 to obtain $q(\theta)$, and then $q(\theta)$ in eq 1 to obtain $\xi(\theta)$, allows the latter quantity to be plotted against $\cos^2\theta$. The diffuse layer potential $\psi[c,q(\theta)]$ in the expression of $\xi(\theta)$ was calculated from the Gouy−Chapman theory and makes only a small contribution to $\xi(\theta)$.

Figure 3 shows $\xi(\theta)$ vs $\cos^2\theta$ plots for all Hg-supported SAMs in 0.1 M KCl. They were obtained by ascribing to q the values estimated from Figure 2 at the appropriate potentials and by setting C_{SAM} equal to 11 μF cm^{-2} for the **3**+ and **3**− SAMs and to 8.5 μF cm^{-2} for the **5**+ and **5**− SAMs. The slopes of the four plots are close. Upon considering the limits of the experimental errors in the estimate of q and C_{SAM} and their propagation in the estimate of the $\xi(\theta)$ function, the surface dipole potential χ for all four SAMs can be estimated at +220 ± 20 mV, positive toward the electrode.

It should be noted that the slope of the $\xi(\theta)$ vs $\cos^2\theta$ plots measures the deviation from the behavior of a parallel plate capacitor. If the SAM molecules point the positive pole of their dipoles toward the electrode (i.e., if μ is positive), a drop expansion decreases the positive potential difference created by the dipole moments as a consequence of their tilt. Consequently, during the drop expansion, a positive charge must flow to the electrode surface along the external circuit to maintain the potential difference across the whole interface constant. This causes the $\xi(\theta)$ function to move in the positive direction with increasing tilt (i.e., with decreasing $\cos^2\theta$), imparting a negative slope to the $\xi(\theta)$ vs $\cos^2\theta$ plot. The linear increase of ξ with a decrease of $\cos^2\theta$ excludes the possibility of a breakdown of the peptide monolayer during the drop expansion.

It has been reported that the Au−S bond can make an appreciable contribution to the surface dipole potential of alkanethiol monolayers[6] and helical peptides[4,8b] tethered to gold. The present procedure, based on the gradual tilt of the tethered thiol molecules, should not produce an appreciable tilt of the Hg−S bond. Therefore, the measured surface dipole potential should not include the contribution from this bond.

Chronocoulometric Charge Density Measurements on the Hg-Supported SAMs. Chronocoulometric measurements of the charge density as a function of the applied potential E were carried out on all four Aib-peptide SAMs immersed in aqueous 0.1 M TMACl. To this end, a series of potential steps was carried out from an initial potential E_i equal to that chosen for q measurements (i.e., $E_i = -0.75$ V for **3**+, **5**+, and **5**− and −0.95 V for **3**−) toward both positive and negative final potentials, E_f, and the resulting charge vs time curves were recorded. Each potential step was preceded by a rest time of 30 s at E_i. The charge transients show an abrupt increase within

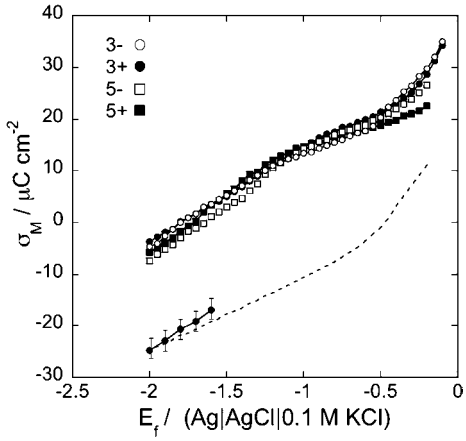

Figure 4. Curves of the total charge density σ_M against E_f obtained from serial charge transients on Hg-supported SAMs of **3**− (open circles), **3**+ (solid circles), **5**− (open squares), and **5**+ (solid squares) in aqueous 0.1 M TMACl. The solid circles with error bars are charge densities obtained from pristine charge transients on a **3**+ SAM. The dashed curve is the σ_M vs E_f plot on bare mercury.

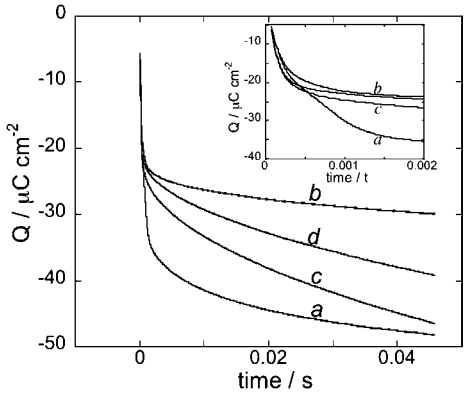

Figure 5. Charge vs time curves obtained by stepping from $E_i = -0.750$ to −1.80 V on newly formed Hg-supported SAMs of **5**+ (curves *a* and *b*) and of **5**− (curves *c* and *d*), in aqueous 0.1 M TMACl; *a* and *c* were obtained from pristine potential steps, *b* and *d* from the immediately subsequent steps. The inset shows the initial portion of the four charge transients, to point out the sigmoidal shape of curve *a*.

a few milliseconds, followed by a slow increase due to the background current. The charge measured immediately after the abrupt increase, once referred to the unit surface, yields $\sigma_M(E_f) - \sigma_M(E_i) \equiv \Delta\sigma_M$. Figure 4 shows the $\Delta\sigma_M$ vs E_f curves for the four SAMs; the curves are shifted along the vertical axis to provide a fairly accurate plot of the total charge density σ_M against E_f, on the basis of the considerations made in the subsequent Discussion section.

The peptides thiolated at the N-terminus (**3**+ and **5**+) exhibit an appreciable difference in the desorption behavior with respect to those thiolated at the C-terminus (**3**− and **5**−). This difference between the **5**+ and **5**− SAMs is shown in Figure 5, but an entirely analogous difference is encountered between the **3**+ and **3**− SAMs. This difference is observed when we carry out the "pristine" potential step on a newly formed SAM-coated mercury drop from E_i to final potentials $E_f \leq -1.60$ V, where the differential capacitance of the **3**+ and **5**+ SAMs coincides with that of bare mercury (see Figure 1). With the Aib-peptides thiolated at the N-terminus, **3**+ and **5**+, the absolute value of the negative charge involved in these pristine potential steps is higher than that involved in the corresponding "serial" steps, namely, the steps yielding the charges reported in Figure 4 (apart

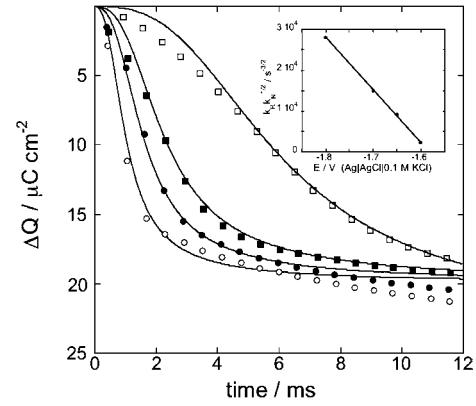

Figure 6. Difference, ΔQ, between the pristine charge transient and the immediately subsequent one on a Hg-supported **5**+ SAM in aqueous 0.1 M TMACl. The charge transients were obtained by stepping from $E_i = -0.75$ V to $E_f = -1.60$ (open squares), −1.65 (solid squares), −1.70 (solid circles), and −1.80 V (open circles). The solid curves were calculated from the model described in the text for $n = 2$, NF $= -2.5$ μC cm^{-2} and for different values of the kinetic parameter $k_R k_N^{1/2}$. This parameter is plotted against the final potential E_f in the inset.

from the five solid circles with error bars at the bottom of the figure). The charge vs time curve following each pristine step exhibits an abrupt increase in charge, which attains a value practically equal to that for the corresponding serial step. This is followed by a sigmoidal charge vs time curve, as shown by curve *a* in the inset of Figure 5, which refers to the **5**+ SAM. All subsequent steps after the pristine one yield a charge vs time curve (see curve *b* in Figure 5) practically equal to that obtained with the corresponding serial step. The height of this sigmoidal curve is about equal to 20 μC cm^{-2} at all final potential values ≤ -1.60 V. This is shown in Figure 6, which reports the difference, ΔQ, between the pristine and the second charge transient on each newly formed drop for the **5**+ SAM, at different values of the final potential E_f.

As distinct from the **3**+ and **5**+ SAMs, the **3**− and **5**− SAMs exhibit a pristine charge transient (see curve *c* in Figure 5) whose initial abrupt rise is almost equal to that of the corresponding serial charge transient. However, the background charge flowing after this abrupt rise increases in time more rapidly than that for the corresponding serial charge transient and, even more so, for the charge transient on the **5**+ SAM. The second and subsequent charge transients after the pristine one (curve *d* in Figure 5) are practically equal to the corresponding serial charge transient.

Similar charge transients were recorded with Hg-supported **5**+ SAMs in aqueous 0.1 M TMAOH + 0.1 M TMACl, where these peptides are present in the anionic, deprotonated form. The only difference consisted in steeper sigmoidal charge vs time curves, under otherwise identical conditions.

4. Discussion

The present extrathermodynamic approach indicates that Hg-supported SAMs of Aib-peptides thiolated at the C-terminus have the same positive surface dipole potential as those thiolated at the N-terminus, within the limits of experimental error. This result is in apparent contrast with the fact that all free peptides herein investigated have the dipole moment directed from the C- to the N-terminus. This behavior can be explained if the strong interfacial electric field created by the negative charge density *q*, experienced by the diffuse layer ions and directed toward the metal, causes an inversion of the dipole moment of

the peptide molecules thiolated at the C-terminus. Since the latter molecules are tightly bound to the mercury surface via the Hg−S bond, this reorientation requires the cleavage of the intramolecular H bonds responsible for the 3_{10}-helix and the formation of intermolecular H-bonds with a favorable orientation of the C═O bond dipole moments. The negative enthalpic contribution from the electrostatic interaction of the latter dipole moments with the interfacial electric field, combined with the positive entropic contribution from the randomized intermolecular H bonds, should more than compensate for the positive enthalpic contribution from the breaking of the more ordered intramolecular H bonds. In other words, a reorientation of the overall dipole moment of tethered peptide molecules thiolated at the C-terminus should be associated with a net decrease in free energy. The formation of intermolecular H bonds at the expense of intramolecular ones is expected to be much less pronounced with tethered peptides thiolated at the N-terminus, in view of the favorable orientation of their "natural" dipole moment with respect to the interfacial electric field.

In addition to the interfacial electric field, E_{ief}, the "endogeneous" electric field created by the natural surface dipole potential of the **3**− and **5**− SAMs may also cooperate in reversing the dipole moment of these peptides. By natural surface dipole potential we mean the dipole potential that the **3**− and **5**− adsorbed molecules would create if they maintained the dipole moment of the isolated molecules. As a rough approximation, this surface dipole potential can be regarded as equal to and opposite that estimated for the **3**+ and **5**+ SAMs, i.e., $\chi = -0.220$ mV. The endogeneous electric field, E_{end}, is given by χ/d, where d is the thickness of the monolayer. Noting that in 3_{10}-helices each amino acid unit determines a structure elongation of ∼2 Å, and using molecular models of such a helical structure, d can be estimated at ∼14 Å for the **3**+ and **3**− peptides and at ∼18 Å for the **5**+ and **5**− peptides. Taking **3**− as an example, E_{end} is equal to 1.57×10^6 V/cm and is directed toward the metal. This electric field is to be compared with the interfacial electric field, which is equal to $E_{ief} \cong q/(\nabla\nabla_0)$. Noting that the differential capacitance of a SAM is given by $C_{SAM} \cong \nabla\nabla_0/d$, we also have $E_{ief} \cong q/(dC_{SAM})$. For the **3**− SAM at −0.95 V, q equals $-6\ \mu$C cm^{-2} and C_{SAM} equals 11 μF cm^{-2}. Hence, E_{ief} is approximately equal to 3.9×10^6 V/cm. Consequently, the interfacial electric field at a negatively charged electrode and the endogeneous electric field are comparable in magnitude and are both directed toward the metal. According to Naaman and co-workers,[5] an endogenous electric field directed toward the metal induces ET from the metal to the adsorbed molecule, thus decreasing its effective dipole moment. However, Naaman's work function measurements were carried out in vacuo, on SAMs of molecules of low polarizability and with no intramolecular hydrogen bonds.[27] Under these conditions, the energetically favored route in response to the endogenous electric field is a charge transfer from the metal. In our case, the **3**− and **5**− SAMs respond to the combined action of the interfacial and the endogenous electric fields through a reorganization of hydrogen bonds, leading to a reversal of the dipole moments.

The fact that the surface dipole potentials of the **5**+ and **5**− SAMs are close to those of the **3**+ and **3**− SAMs suggests that the longer peptides are more tilted than the shorter ones on an unexpanded mercury drop. This is also confirmed by the ratio of the differential capacitance of the **5**+ and **5**− SAMs to that of the **3**+ and **3**− SAMs being about equal to 8.5/11 ≅ 3/4: for an equal value of the dielectric constant for all SAMs, such a ratio should be equal to 3/5.

When long-chain thiols undergo deprotonation upon chemisorption on noble metals, they generate a negative charge in contact with the electrode surface. In such a case, they may transfer their negative charge to the electrode. However, the long chain of thiols in SAMs has a dual effect: (i) It interposes a thick slab of high resistance and low capacitance between the sulfhydryl functional group and the bulk aqueous phase. This makes any charge movement from the functional group to the metal surface hardly appreciable with respect to the bulk phase. (ii) It decreases the screening of the negative charge of the functional groups by diffuse layer ions down to a negligible extent.[28] Consequently, this negative charge must be compensated for by an almost equal and opposite charge on the electrode surface to maintain the electroneutrality of the electrified interface, independent of whether partial or total charge transfer from the functional group to the electrode takes place or not.[10,29] This implies that a high positive charge density σ_M on the electrode surface following the self-assembly of a thiol or disulfide monolayer does not allow us to establish whether total, partial, or no charge transfer takes place.

The fact that the pristine charge transients for **3**+ and **5**+ SAMs are higher than the corresponding serial charge transients can be explained by assuming that, on a newly formed SAM, the sulfhydryl groups are totally deprotonated at the initial potential E_i, independent of the extent of partial charge transfer. During the series of potential steps yielding the charge vs potential curves in Figure 4, the Hg−S bonds are progressively broken, with protonation of the resulting sulfide groups, as the final potential E_f is made sufficiently negative. For these negative E_f values, the subsequent backward $E_f \rightarrow E_i$ potential step causes the readsorption of the protonated peptides; consequently, the charge density $\sigma_M(E_i)$ becomes progressively less positive, to maintain the electroneutrality of the interface. Ultimately, for sufficiently negative E_f values, all the initial negative charge associated with the SAM of deprotonated thiopeptides is lost, and the negative charge density involved in the forward $E_i \rightarrow E_f$ potential step is decreased by the same amount. This explains why the pristine charge transients following all potential steps from E_i to E_f values ≤ −1.60 V are more negative than the corresponding serial charge transients by about the same amount of $-20\ \mu$C cm^{-2}. In aqueous 0.1 M TMAOH + 0.1 M TMACl, where the thiolated Aib-peptides are expected to be deprotonated, the role of protons after Hg−S cleavage can also be played by K^+ or Na^+ cations, which may reach the electrode surface through the partially disorganized SAM.

By using the unit cell size of pBrBz−$(Aib)_{10}$−O*t*Bu or *Z*-$(Aib)_{11}$−O*t*Bu estimated by X-ray analysis,[30] the diameter of helical Aib-peptides can be set equal to 9.7 Å. By assuming that the peptide helixes are impenetrable cylinders forming a hexagonal compact lattice, with the helix axis normal to the electrode surface, the cross sectional area of a helix is estimated at $3^{1/2}d^2/2 = 81.5$ Å^2. If we ascribe a single electronic charge

(27) Cahen, D.; Naaman, R.; Vager, Z. *Adv. Funct. Mater.* **2005**, *15*, 1571–1578.

(28) Becucci, L.; Guidelli, R. *Soft Matter* **2009**, *5*, 2294–2301.

(29) Kunze, J.; Leitch, J.; Schwan, A. L.; Faragher, R. J.; Naumann, R.; Schiller, S.; Knoll, W.; Dutcher, J. R.; Lipkowski, J. *Langmuir* **2006**, *22*, 5509–5519.

(30) (a) Toniolo, C.; Crisma, M.; Bonora, G. M.; Benedetti, E.; Di Blasio, B.; Pavone, V.; Pedone, C.; Santini, A. *Biopolymers* **1991**, *31*, 129–138. (b) Gessmann, R.; Bruckner, H.; Petratos, K. *J. Pept. Sci.* **2003**, *9*, 753–762.

to each helix, a charge density of 23.4 μC cm^{-2} is estimated for desorption of a tightly packed Aib-peptide SAM. This supports the view that the excess charge of pristine charge transients over the corresponding serial ones is due to desorption of a deprotonated compact SAM of **3**+ or **5**+ peptide. The fact that the same excess charge is observed with the **3**+ and **5**+ SAMs indicates that the two SAMs have practically the same surface coverage, even though the closeness of their differential capacities and surface dipole potentials suggests that the molecules of the **5**+ SAM are more tilted than those of the **3**+ SAM.

The sigmoidal ΔQ vs time curves in Figure 6 are reminiscent of a nucleation and growth process. We can envisage such a process as follows. Since the detachment of the thiolated peptide molecules from the electrode surface requires Hg−S bond cleavage and sulfide group reprotonation, we will briefly refer to these molecules as "bound" or "unbound", depending on whether they maintain the Hg−S bond or not. The breaking of the Hg−S bond of a single thiolated peptide may not be sufficient to allow its detachment from the electrode surface, since it is surrounded by molecules H-bonded to it. Clusters of contiguous unbound thiopeptide molecules can be regarded as characterized by a critical size, called "nucleus". Below this critical size, the molecules will have a higher tendency to form again Hg−S bonds than to induce other neighboring bound molecules to break their Hg−S bonds with a resulting increase in cluster size. Conversely, above this critical size, the unbound clusters will have a practically irreversible tendency to grow.

This nucleation and growth process can be treated using a model developed in ref 31 and based on the Avrami formalism. Let us denote by Φ the fraction of the unit surface area of the SAM covered by bound thiolated peptides and by Φ_0 its initial value, before the start of nucleation and growth; clearly, Φ_0 is equal to unity. According to the kinetic model of nucleation and growth of ref 31, the nucleation rate can be written

$$dN/dt = k_N\Phi^n \qquad (3)$$

Here, N is the number of nuclei per unit surface area, k_N is the nucleation rate constant, and n is the number of the unbound peptide molecules composing a critical nucleus. Let us assume for simplicity that the growing supercritical clusters have a circular shape, of radius r. Moreover, let the rate of radial growth of these clusters be proportional to the probability, $2\pi r\Phi$, of bound molecules being adjacent to the perimeter of the unbound cluster. With these assumptions, the growth rate is given by

$$\frac{d}{dt}(\pi r^2) = 2\pi r\frac{dr}{dt} = k_R 2\pi r\Phi \rightarrow \frac{dr}{dt} = k_R\Phi \qquad (4)$$

where k_R is the rate constant of radial growth. Starting from eqs 3 and 4, the kinetic model involves the numerical solution of five differential equations. Fitting the calculated $\Delta Q(t)$ vs t curves to the corresponding experimental curves (see Figure 6) at different applied potentials E_f requires two free parameters, apart from a potential-independent normalizing factor, NF. They are the number n of unbound peptide molecules composing a nucleus and the potential-dependent product $k_R k_N^{1/2}$, which summarizes the kinetic features of the whole nucleation and growth process. Thus, identical results are obtained with k_R much lower, equal, or much higher than k_N, provided that the $k_R k_N^{1/2}$ product is the same. Therefore, this model may account for the formation both of small dispersed clusters, when the rate constant of nucleation is higher than that of radial growth, and of larger aggregates in the opposite case. Figure 6 shows the experimental $\Delta Q(t,E)$ vs t plots at different potentials together with the corresponding curves calculated for NF = −2.5 μC cm^{-2}, $n = 2$, and for different values of $k_R k_N^{1/2}$. The inset of the figure shows the linear dependence of the overall rate constant $k_R k_N^{1/2}$ upon the applied potential E_f. Such a linear dependence is to be related to the electrostatic interaction between the interfacial electric field and the water dipoles, which gradually displace the SAM molecules from the direct contact with the mercury surface. When the water dipoles are fully aligned with their positive end toward the electrode, this electrostatic interaction is proportional to the interfacial electric field, which varies linearly with E.

The above interpretation of the nucleation and growth process may provide an explanation for the lack of desorption of the **3**− and **5**− SAMs, even at the most negative experimentally accessible potentials. The reversal in the natural dipole moment of these thiolated peptides, as imposed by the interfacial electric field, causes these molecules to be much more intermolecularly H-bonded than the **3**+ and **5**+ molecules. This makes their complete detachment from the electrode surface much more difficult. Moreover, the intercalation of water molecules among the **3**− and **5**− molecules at far negative potentials, and their close vicinity to the sulfide groups, may catalyze a modest hydrogen evolution; this explains the higher slope of the charge transients of the **5**− SAM (curves *c* and *d* in Figure 5) with respect to those of the **5**+ SAM (curves *a* and *b* in Figure 5), after the initial abrupt flow of capacitive charge.

In Figure 4, all the $\Delta\sigma_M$ vs E_f plots obtained from the serial potential steps are shifted along the vertical axis by an amount equal to $(20 + q)$ μC cm^{-2}, where q is the negative charge experienced by the diffuse layer ions at the initial potential E_i, at which $\Delta\sigma_M$ is equal to zero. The rationale behind this shift is as follows. We assume that the charge density associated with the SAMs of all four deprotonated thiolated peptides, including the **3**− and **5**− SAMs, is equal to −20 μC cm^{-2}. Independent of whether this charge is totally, partially, or not transferred to the electrode at E_i, a potential step from E_i to a final potential E_f negative enough to cause complete thiolated peptide desorption would release this charge. Incidentally, such a potential step is actually realized for the **3**+ and **5**+ SAMs, whereas it is not realizable for the **3**− and **5**− SAMs. Since the diffuse layer ions experience a charge density q at E_i, the charge density involved in such an $E_i \rightarrow E_f$ potential step is equal to $\sigma_M(E_f) - (20 + q)$ μF cm^{-2}, where $\sigma_M(E_f)$ is the total charge density at E_f on a bare mercury electrode. Therefore, the vertical shift of the $\Delta\sigma_M$ vs E_f plots in Figure 3 by $(20 + q)$ μC cm^{-2} serves to position them with respect to the vertical axis of the total charge density σ_M.

The closeness of the estimated surface dipole potentials of the present Hg-supported Aib-peptide SAMs thiolated at the C- and N-termini is in apparent contrast with opposite effects that Au-supported peptide SAMs thiolated at the opposite termini exert upon a number of electrochemically[8,9] and photoelectrochemically[3c,d] induced electron-transfer processes. However, the endogeneous electric field created on peptides by a positively charged N-terminus and a negatively charged C-terminus has often been found to favor peptide conformations with the dipole directed toward the C-terminus and to destabilize conformations with the dipole directed toward the N-terminus.

(31) Becucci, L.; Moncelli, M. R.; Guidelli, R. *J. Am. Chem. Soc.* **2003**, *125*, 3785–3792.

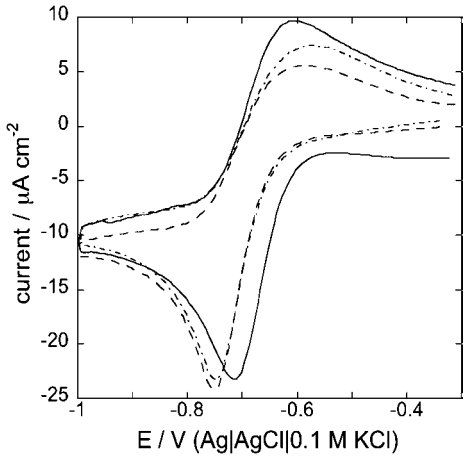

Figure 7. Cyclic voltammogram of 1×10^{-4} M Eu(III) in 0.1 M KCl on bare mercury (solid curve) and on mercury coated with a **5**+ (dashed curve) and a **5**− SAM (dash−point curve). Scan rate: 50 mV/s.

This trend has been observed both with oligoprolines,[32] where no hydrogen bonds are involved, and with certain α- and β-peptides.[32−34]

To verify the effect of the present Hg-supported SAMs upon a simple redox process taking place over the potential range of maximum stability of the SAMs, the cyclic voltammograms of Eu(III) in aqueous 0.1 M KCl were recorded on bare mercury as well as on mercury coated with **5**+ and **5**− SAMs. The cyclic voltammogram of the Eu(III)/Eu(II) redox couple in 0.1 M KCl is quasi-reversible, with a formal potential of −0.657 V. Its peak potential varies linearly with the square root of the potential scan rate, denoting mixed control by diffusion and ET. Figure 7 shows that coating the mercury electrode with the Aib-peptide SAMs does not depress the voltammetric peak currents. Since the film is compact, as we already commented upon, this outcome denotes high electron-conduction properties of these peptides and is in keeping with our previous results in solution, obtained with donor−peptide−acceptor systems, showing that Aib chains mediate electron tunneling very efficiently.[13] The **5**+ and **5**− SAMs exert a similar effect on the voltammetric behavior of the Eu(III)/Eu(II) redox couple. Both coatings make the oxidation peak flatter and more rounded; moreover, they cause a negative shift of the reduction peak potential by 35−37 mV and of the midpoint potential by 8−12 mV. These effects are modest. However, under the reasonable assumption that they are due to the surface dipole potentials of the **5**+ and **5**− SAMs, they confirm that these dipole potentials act in the same direction. Similar effects on the Eu(III)/Eu(II) couple are exerted by the **3**+ and **3**− SAMs on mercury (data not shown).

The opposite effects that Au-supported SAMs of peptides thiolated at the C- and N-terminus, respectively, have sometimes shown to exert on electrochemical and photoelectrochemical processes cannot be directly compared with the present results on Hg-supported peptide SAMs. In fact, the direction and magnitude of the interfacial electric field on Au-supported SAMs is usually not known. In addition, an intrinsic difference between Hg-supported and Au-supported peptide SAMs should be stressed. The liquid nature of mercury imparts a high degree of lateral mobility and axial rotation to the tethered peptide molecules during film stabilization. The formation of an Aib peptide SAM on mercury requires about 90 min of immersion in its ethanol solution. Conversely, we found that the formation of SAMs of the same thiolated peptides on gold requires at least 48 h.[18] In other words, the fluid nature of mercury is envisaged as important for allowing conformational modifications of these peptides upon electrode polarization.

5. Conclusions

By taking advantage of the liquid nature of mercury, it was possible to estimate the surface dipole potential of self-assembled monolayers of four oligopeptides consisting of a sequence of α-aminoisobutyric acid units, thiolated at either the N- or C-terminus by means of a $-(CH_2)_2-SH$ anchor. To this end, a novel procedure combining mercury drop expansion and diffuse layer capacitance measurements was adopted. While the above peptides adopt a robust 3_{10}-helix conformation both in solution and in the solid state, our results indicate that the situation may be quite different when they are tightly assembled onto a mercury surface: when the interfacial electric field is sufficiently strong and the direction of the field contrasts the natural molecular dipole moment associated with the 3_{10}-helix, the peptides may be forced to change the direction of the dipole, which implies a very substantial conformational change. The endogeneous electric field created by Aib-peptides thiolated at the C-terminus and tethered to mercury with their natural dipole moment may also cooperate with the interfacial electric field in inverting the direction of the surface dipole potential.

The strength of this study rests in providing experimental evidence that significantly enhances our understanding of how molecules possessing a strong dipole moment may react toward imposition of an electric field while anchored to a metal surface; this is particularly relevant in areas such as sensors, molecular electronics, and nanosystems. Intriguing questions are also raised about possible peptide conformational changes under severe conditions, which could be important to better understand the mechanism of long-range electron transfers occurring in biological systems, such as redox proteins on electrodes.

Acknowledgment. The financial support by Ente Cassa di Risparmio di Firenze and that by the Italian Ministero dell'Istruzione, dell'Università e della Ricerca (MIUR) through PRIN 20079Y9578, are gratefully acknowledged.

JA100486Y

(32) Kuemin, M.; Schweizer, S.; Ochsenfeld, C.; Wennemers, H. *J. Am. Chem. Soc.* **2009**, *131*, 15474–15482, and references therein.
(33) Fairman, R.; Shoemaker, K. R.; York, E. J.; Stewart, J. M.; Baldwin, R. L. *Proteins* **1989**, *5*, 1–7.
(34) Hart, S. A.; Bahadoor, A. B. F.; Matthews, E. E.; Qiu, X. J.; Schepartz, A. *J. Am. Chem. Soc.* **2003**, *125*, 4022–4023.